

**Search for supersymmetry using boosted Higgs bosons and  
missing transverse momentum in proton-proton collisions**  
**at 13 TeV**

by

**Frank Jensen**

M.S., University of Colorado Boulder, 2014

B.A., University of California Berkeley, 2008

A thesis submitted to the  
Faculty of the Graduate School of the  
University of Colorado in partial fulfillment  
of the requirements for the degree of  
Doctor of Philosophy  
Department of Physics

2018

This thesis entitled:  
Search for supersymmetry using boosted Higgs bosons and missing transverse momentum in  
proton-proton collisions at 13 TeV  
written by Frank Jensen  
has been approved for the Department of Physics

---

Professor Kevin Stenson

---

Professor William Ford

---

Professor Jamie Nagle

---

Professor John Cumalat

---

Professor Senarath de Alwis

Date \_\_\_\_\_

The final copy of this thesis has been examined by the signatories, and we find that both the content and the form meet acceptable presentation standards of scholarly work in the above mentioned discipline.

Jensen, Frank (Ph.D.,experimental high-energy physics)

Search for supersymmetry using boosted Higgs bosons and missing transverse momentum in proton-proton collisions at 13 TeV

Thesis directed by Professor Kevin Stenson

A search for physics beyond the Standard Model in events with one or more high-momentum Higgs bosons,  $H$ , decaying to pairs of  $b$  quarks in association with missing transverse momentum is presented. The data, corresponding to an integrated luminosity of  $35.9 \text{ fb}^{-1}$ , were collected with the CMS detector at the LHC in proton-proton collisions at the center-of-mass energy  $\sqrt{s} = 13 \text{ TeV}$ . The analysis utilizes a new  $b$  quark tagging technique based on jet substructure to identify jets from  $H \rightarrow b\bar{b}$ . Events are categorized by the multiplicity of  $H$ -tagged jets, jet mass, and the missing transverse momentum. No significant deviation from standard model expectations is observed. In the context of supersymmetry (SUSY), limits on the cross sections of pair-produced gluinos are set, assuming that gluinos decay to quark pairs,  $H$  (or  $Z$ ), and the lightest SUSY particle, LSP, through an intermediate next-to-lightest SUSY particle, NLSP. With large mass splitting between the NLSP and LSP, and 100% NLSP branching fraction to  $H$ , the lower limit on the gluino mass is found to be 2010 GeV.

## **Dedications**

The taxpayers.

## Contents

### Chapter

<b>1</b>	<b>Introduction</b>	<b>1</b>
<b>2</b>	<b>The Standard Model of Particle Physics</b>	<b>2</b>
<b>3</b>	<b>The CMS Detector</b>	<b>3</b>
3.1	Silicon Tracker . . . . .	5
3.2	Electromagnetic Calorimeter . . . . .	5
3.3	Hadronic Calorimeter . . . . .	5
3.4	Solenoidal Magnet . . . . .	5
3.5	Muon System . . . . .	5
3.6	Particle Flow Event Reconstruction . . . . .	5
3.7	Trigger System . . . . .	5
<b>4</b>	<b>Analysis</b>	<b>6</b>
4.1	Introduction . . . . .	6
4.2	Event & Object Selection . . . . .	6
4.3	Background Estimation Procedure . . . . .	7
4.4	Results . . . . .	8
<b>5</b>	<b>Conclusions</b>	<b>13</b>



## Tables

### Table

4.1	Yields in each of the 6 analysis regions. . . . .	9
4.2	Observed yields in signal and control regions, along with the background predictions.	10

## Figures

### Figure

3.1	A depiction of the CMS detector. . . . .	3
3.2	A schematic view of the CMS detector and the particles it interacts with. . . . .	4
4.1	A diagram of the SMS models used for interpretations of this analysis. . . . .	7
4.2	A diagram of the partitioned phase space. . . . .	8
4.3	Simulation-based closure in the signal regions. . . . .	9
4.4	Observed yields in the single and double Higgs-tagged signal regions. . . . .	10
4.5	Observed and expected limits on the gluino cross section when the data are interpreted in the T5HH and T5HZ models. . . . .	12

## **Chapter 1**

### **Introduction**

A description of the Standard Model is presented in Chapter 2. A description of the CMS detector is presented in Chapter 3. A description of the physics analysis is presented in Chapter 4. The conclusions are discussed in Chapter 5.

## **Chapter 2**

### **The Standard Model of Particle Physics**

A section describing the Standard Model of particle physics.

## Chapter 3

### The CMS Detector

The detector is cylindrically symmetric, with a modular design consisting of different subsystems specialized for detection or identification of specific particles. Many of the Standard Model particles are unstable. In fact only about 8 particles are directly detected in our experiment, the rest of those being reconstructed via their decay into these more stable elements. Of all the Standard Model particles,

Figure 3.1 is a depiction of the CMS detector. Figure 3.2 is a schematic view of the CMS detector and the particles it interacts with.

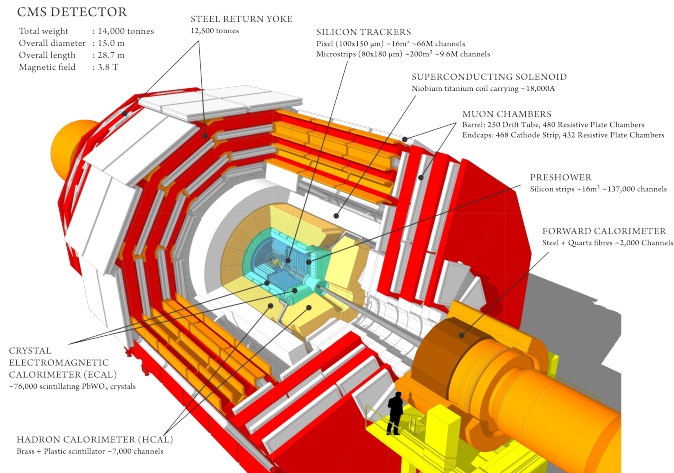


Figure 3.1: A depiction of the CMS detector.

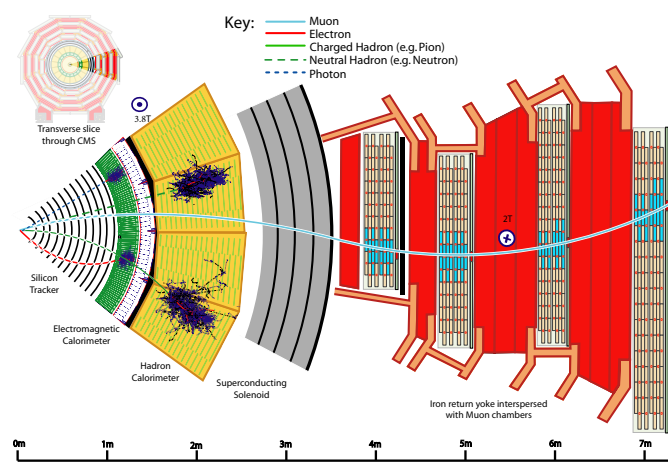


Figure 3.2: A schematic view of the CMS detector and the particles it interacts with.

### **3.1 Silicon Tracker**

At the center of the detector lies the silicon tracker which is responsible for momentum reconstruction of charged particles and reconstruction of the primary vertices created from a proton-proton interaction. The tracker is composed of a number of concentric cylindrical layers each instrumented with silicon sensors. As a charged particle traverses an individual sensor a small amount of ionization energy is deposited in that element. A bias voltage is applied across the sensor to direct the charge to either end of the sensor. Bonded to the sensors are front-end electronics responsible for the amplification and shaping of the resultant signal. Neighboring elements are clustered together creating what is known as a “hit”. These hits are then used to reconstruct the particle’s trajectory through the tracker. To make a measurement of the momentum and charge of the particle, the tracker is immersed in a 3.8 T magnetic field which bends the trajectory of the particle.

The tracker is further divided into an inner and outer parts which make use of slightly different technologies. The inner part of the tracker is known as the pixel detector and consists of 4 layers which the sensitive elements are silicon pixels of size  $100 \times 150 \mu\text{m}$ . This fine granularity of

### **3.2 Electromagnetic Calorimeter**

### **3.3 Hadronic Calorimeter**

### **3.4 Solenoidal Magnet**

### **3.5 Muon System**

### **3.6 Particle Flow Event Reconstruction**

Particle Flow event reconstruction is pretty good.[1]

### **3.7 Trigger System**

## Chapter 4

### Analysis

#### 4.1 Introduction

As the search for Supersymmetry continues to come up empty handed, the masses of potentially new particles are pushed to larger and larger scales. One consequence is that the Standard Model particles radiated in their decay should have correspondingly larger and larger momentum. As the momentum of a particle becomes larger the decay products tend to be emitted at smaller angles, eventually reaching the point where we could reconstruct all the decay objects within a single “fat jet” reconstructed using the “anti- $k_t$ ” algorithm with a cone size parameter 0.8. We present an analysis searching for hints of new physics beyond the Standard Model in events with one or two Higgs bosons and a large imbalance in the transverse momentum resulting from supersymmetric particles escaping detection. We require the Higgs boson to decay to b-quarks, exploiting the large (57%) branching fraction to b-quarks. The branching fraction of Z bosons to b-quarks is substantially smaller at 15%. This analysis built heavily on previously published work [2] [3]. To further suppress misidentification of these jets, we further require the invariant mass of the jet to be consistent with the Higgs boson, to improve mass reconstruction, the soft and wide angle radiation is first removed from the jet before the mass calculation.

#### 4.2 Event & Object Selection

Although our analysis is sensitive to any process which can produce boosted Higgs or Z bosons, we have adopted a couple of benchmark models, seen in Figure 4.1, to give motivation to

the region of phase space we work in. In this scenario, the proton-proton interaction produces a pair of gluinos ( $\tilde{g}$ ) which decay to a neutralino ( $\chi_2^0$ ) by the emission of Standard Model quarks. A small mass splitting between the gluino and neutralino ( $\chi_2^0$ ) will result in low  $p_T$  quarks and a high  $p_T$  neutralino  $\chi_2^0$ . This neutralino  $\chi_2^0$  further decays into another neutralino  $\chi_1^0$  with the emission of a Higgs or Z boson. The neutralino  $\chi_1^0$  escapes detection.

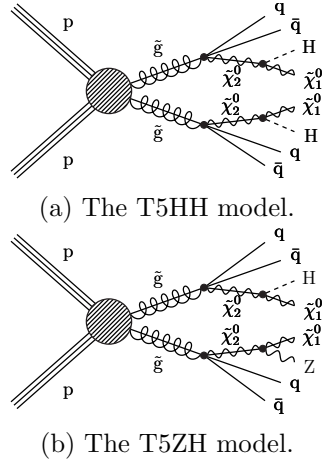


Figure 4.1: A diagram of the SMS models used for interpretations of this analysis.

The most salient selection criteria is the requirement of at least two high- $p_T$  ( $> 300 \text{ GeV}$ ) AK8 jets.

### 4.3 Background Estimation Procedure

The background estimation procedure makes use of what is known as an “ABCD” prediction where the analysis phase space is divided up into signal and sideband regions using scaling relations to make predictions of the Standard Model background inclusive in all processes. The phase space is divided up according to whether or not the jets are a) in the signal mass region and b) have been tagged as being consistent with a  $b\bar{b}$  jet. A diagram of this partitioning is seen in Figure 4.2. The two signal regions  $A_1$  and  $A_2$  contain events with one (and only one) or two jets being consistent with Higgs boson decay. Assuming that there is no correlation between the jet mass and the  $b\bar{b}$ -tagging, the ratio of events  $A_{1,2}/B_{1,2}$  should be the same as C/D. Rearranging this gives a

prediction for the events in the A1 or A2 signal regions,  $(A_{1,2})_{\text{prediction}} = (B_{1,2} * C/D)_{\text{observed}}$ . The signal regions in data are blinded until the background prediction is made, but we are able to test the closure of our background estimation method in simulation. The closure is seen in Figure 4.3. To account for the non-closure in the signal regions in data a correction factor  $\kappa$  is applied to each prediction. The values of  $\kappa$  are calculated from a combination of data and simulation. The values can be seen in Table 4.2.

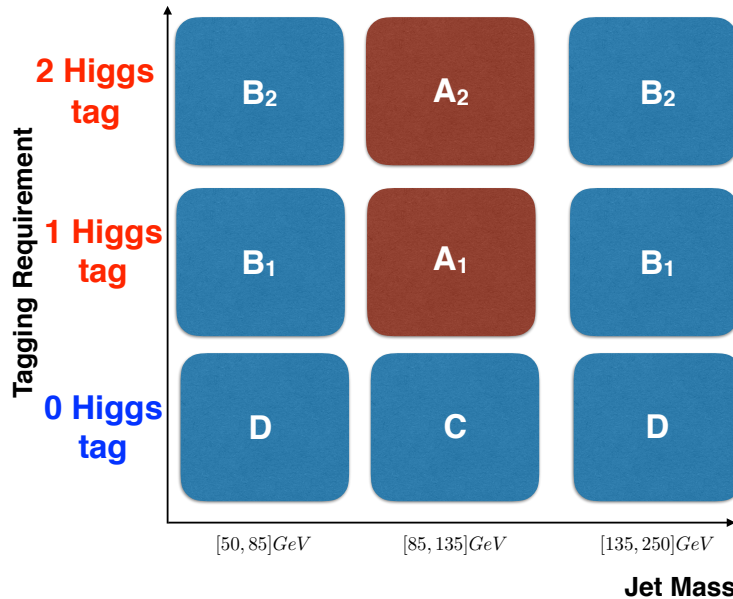


Figure 4.2: A diagram of the partitioned phase space.

Yields in these control regions are seen in Figure 4.2, in addition the the yields in the two signal regions.

#### 4.4 Results

Observed yields in the two signal regions (A1 & A2) are seen in Figure 4.4. Our signal region yields are consistent with the background expectation.

Interpreting our results in the context of the T5HH or T5ZH models, the absence of signal

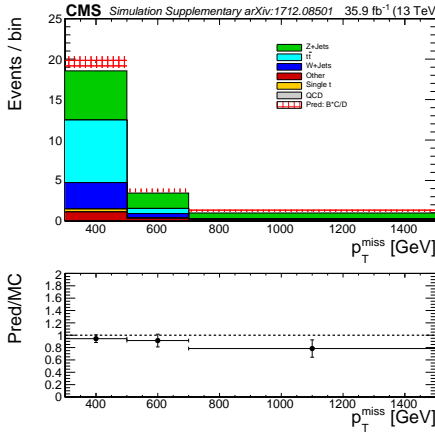
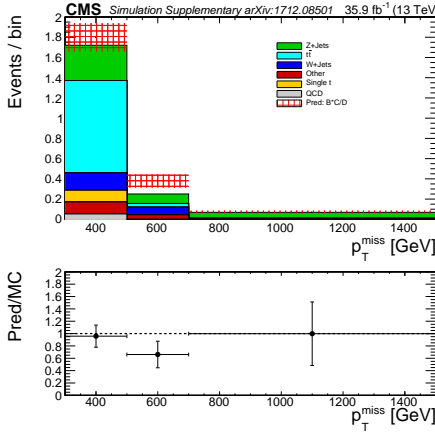
(a) The single Higgs tag region ( $A_1$ ).(b) The double Higgs tag region ( $A_2$ ).

Figure 4.3: Simulation-based closure in the signal regions.

Table 4.1: Yields in each of the 6 analysis regions.

$N_H$	$p_T^{\text{miss}}$ (GeV)	$\kappa$	$A_{\text{predicted}}$	A	B	C	D
1	300 – 500	$0.98 \pm 0.11$	$17.7 \pm 3.8$	15	112	44	273
1	500 – 700	$0.86 \pm 0.16$	$3.4 \pm 1.5$	2	20	12	60
1	>700	$0.86 \pm 0.17$	$0.61 \pm 0.45$	1	5	4	28
2	300 – 500	$0.73 \pm 0.14$	$1.52 \pm 0.57$	1	13	44	273
2	500 – 700	$0.43 \pm 0.12$	$0.09 \pm 0.08$	0	1	12	60
2	>700	$0.62 \pm 0.30$	$0.09^{+0.11}_{-0.09}$	0	1	4	28

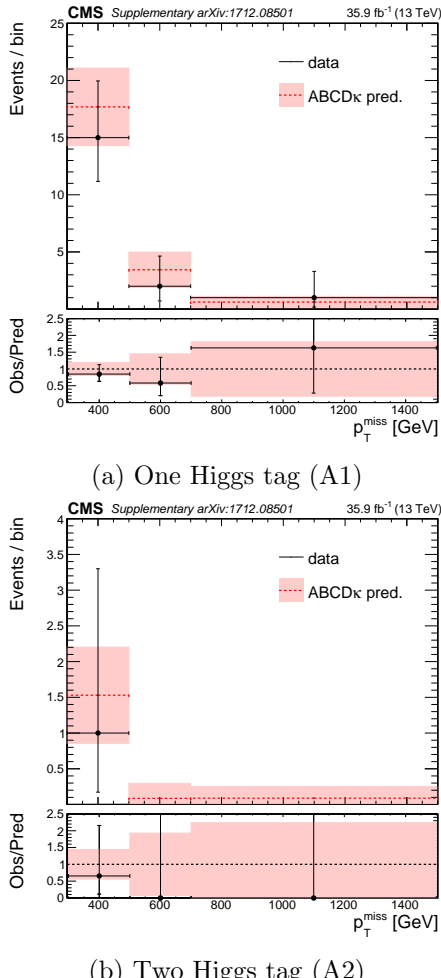


Figure 4.4: Observed yields in the single and double Higgs-tagged signal regions.

Table 4.2: Observed yields in signal and control regions, along with the background predictions.

$N_H$	$p_T^{\text{miss}}$ (GeV)	$\kappa$	$A_{\text{predicted}}$	A	B	C	D
1	300 – 500	$0.98 \pm 0.11$	$17.7 \pm 3.8$	15	112	44	273
1	500 – 700	$0.86 \pm 0.16$	$3.4 \pm 1.5$	2	20	12	60
1	>700	$0.86 \pm 0.17$	$0.61 \pm 0.45$	1	5	4	28
2	300 – 500	$0.73 \pm 0.14$	$1.52 \pm 0.57$	1	13	44	273
2	500 – 700	$0.43 \pm 0.12$	$0.09 \pm 0.08$	0	1	12	60
2	>700	$0.62 \pm 0.30$	$0.09^{+0.11}_{-0.09}$	0	1	4	28

allows us to place limits on the masses of the Supersymmetric particles. Assuming a mass of 1 GeV for the neutralino  $\chi_1^0$ , and a small mass splitting of 50 GeV between the gluino and neutralino  $\chi_2^0$ , we are able to place lower limits at 95% confidence level on the gluino mass at 2010 and 1825 GeV for the T5HH and T5ZH models, respectively. The exclusion curves are seen in Figure 4.5. The weaker limit for the T5ZH model is due to the smaller branching fraction of the Z boson to b-quarks and our choice of signal mass window not being optimal for a Z boson.

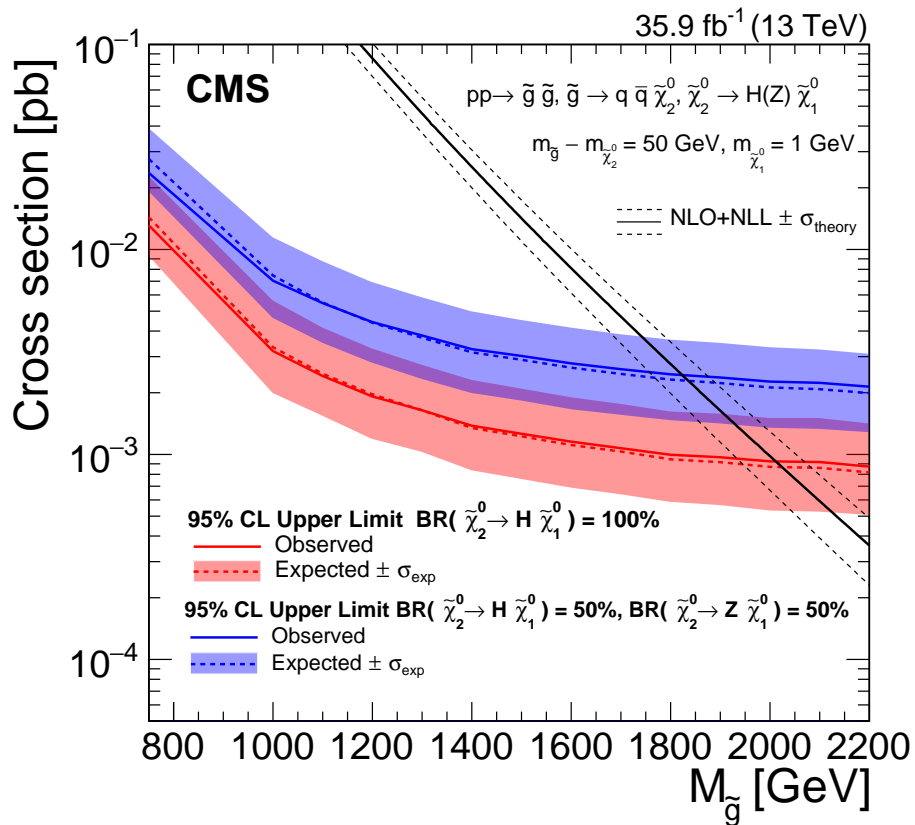


Figure 4.5: Observed and expected limits on the gluino cross section when the data are interpreted in the T5HH and T5HZ models.

## **Chapter 5**

### **Conclusions**

A chapter describing the conclusions. The analysis presented in this thesis is complete and has been published in a peer-reviewed journal[4].

## Bibliography

- [1] A. M. Sirunyan et al., “Particle-flow reconstruction and global event description with the cms detector,” JINST, vol. 12, p. P10003, 2017.
- [2] CMS Collaboration, “Search for supersymmetry in multijet events with missing transverse momentum in proton-proton collisions at 13 tev,” Phys. Rev. D, vol. 96, p. 032003, 2017.
- [3] CMS Collaboration, “Search for supersymmetry in the multijet and missing transverse momentum final state in pp collisions at 13 tev,” Phys. Lett. B, vol. 758, p. 152, 2016.
- [4] CMS Collaboration, “Search for physics beyond the standard model in events with high-momentum higgs bosons and missing transverse momentum in proton-proton collisions at 13 tev,” Phys. Rev. Lett., vol. 120, p. 241801, 2018.